Proceedings of the ASME 2023
International Design Engineering Technical Conferences and
Computers and Information in Engineering Conference
IDETC/CIE2023
August 20-23, 2023, Boston, Massachusetts

DETC2023-XXXXXX

MULTI-MATERIAL AND MULTI-JOINT TOPOLOGY OPTIMIZATION CONSIDERING MULTIPLE DESIGN SPACES

Il Yong Kim[1*], Yuhao Huang[1], Luke Crispo[1]
[1]Queen's University, Kingston, ON, Canada
*kimiy@queensu.ca

ABSTRACT

Today, automakers are focusing on cost reduction and lightweighting, by utilizing a combination of different materials in the vehicle design. Topology optimization is a numerical tool that provides more design freedom than other methods, such as size optimization and shape optimization. Multi-material topology optimization can optimize both material layout and material distribution to improve structural performance. However, these methods assume that dissimilar materials are perfectly bonded, which limits the manufacturability of the design. This work presents a multi-material and multi-joint topology optimization methodology that considers additional design variables for joints in the material interface region. The mechanical properties of joints are included in the analysis, which affects the overall structural behavior and the optimized result. This paper firstly introduces topology optimization methods and material interpolation functions for multiple design spaces. Then, the material interface region detection method is explained. After that, sensitivity analysis for different responses is conducted. Lastly, the results of some example models demonstrate this methodology can be used to control mass and joining cost in multiple design spaces within a structure.

Keywords: Multi-material topology optimization; multi-joint topology optimization; joint design; structural optimization

1. INTRODUCTION

Topology optimization (TO) has become an active research area in both academic and industry since the introduction by Bendsøe and Kikuchi in 1988 [1]. TO is a numerical tool used to determine the (local) optimal material distribution within the design space for certain problem statements. In the density approach, the design variables are the pseudo density of each element and ranged between 0 and 1, where 0 indicates a void element and 1 indicates a solid element. The solid isotropic material with penalization (SIMP) method is used to interpolate material properties from void to solid [2]. Single material topology optimization (SMTO) can be extended to multi-material topology optimization (MMTO) to improve design freedom, and therefore yield better solutions. However, MMTO assumes that the interface between dissimilar materials is perfectly bonded together, which is not realistic from a manufacturing perspective. Shah et al. added a cost constraint for interface regions, but the mechanical properties of joints were not simulated [3]. The first work that considered joint mechanical properties was done by Woischwill and Kim, where the optimization was decomposed into two subproblems, MMTO and multi-joint topology optimization (MJTO) [4]. However, this method was limited to 2D geometry. Florea et al. extended this method to 3D geometry and considered tooling accessibility constraints [5]. However, the methods used by Woischwill and Kim, and Florea et al. had two limitations. Firstly, a specialized finite element mesh was required. Secondly, the optimization process was decoupled into MMTO and MJTO, which was not a simultaneous multi-material and multi-joint topology optimization (MM-MJ-TO). Theoretically, simultaneous optimization would converge to a better result, compared to decoupled optimization. After that, Florea et al. integrated spatial gradient into SIMP formulation and developed simultaneous MM-MJ-TO [6]. In this method, a specialized mesh was not needed. Also, Florea et al. demonstrated a strong dependence between optimal joint design and optimal structural material design. Crispo et al. proposed a new spatial gradient computation method and studied the effect of joint costs on the structural material distribution [7].

The previous MM-MJ-TO framework was limited to single design space. However, industry models often contain multiple design spaces. This paper extends the MM-MJ-TO framework to

multiple design spaces, which allows users to control the distribution of the material and joint cost fractions in different locations within the structure.

2. MATERIALS AND METHODS

2.1 Problem Statement

The problem statement for MM-MJ-TO is shown in (1). The objective is to minimize total compliance of all elements $C(\underset{\sim}{x})$, and the problem is subjected to a set of mass fraction constraints $g_i^1(\underset{\sim}{x})$ and joint cost fraction constraints $g_i^2(\underset{\sim}{x})$. The design variables will control the layout and distribution of two structural materials and two joint materials. Where material 1 and material 2 are the stiffer and weaker structural material candidates, respectively; and material 3 and material 4 are the stiffer and weaker joint material candidates respectively. The geometry is discretized into a finite number of elements. In the designable regions, each element has four design variables, where x_j^1 and x_j^2 determine the existence and selection of structural materials, respectively; x_j^3 and x_j^4 determine the existence and selection of joint materials, respectively.

$$
\begin{aligned}
\underset{\underset{\sim}{x}}{\text{minimize}} \quad & C(\underset{\sim}{x}) = \underset{\sim}{u}^T \underset{\sim}{K} \underset{\sim}{u} \\
\text{subject to} \quad & \underset{\sim}{K}\underset{\sim}{u} = \underset{\sim}{f} \\
& g_i^1(\underset{\sim}{x}) = \frac{1}{\sum_{j\in N_i} v_j \rho^1} \sum_{j\in N_i} \left(v_j \sum_{k=1}^{4} w_j^k \rho^k \right) \le \bar{M}_i \\
& g_i^2(\underset{\sim}{x}) = \frac{1}{\sum_{j\in N_i} v_j} \sum_{j\in N_i} \left(v_j \sum_{k=3}^{4} w_j^k q^k \right) \le \bar{Q}_i \\
& x_j^k \in (0,1], \; k = 1,2,3,4 \\
& i = 1,...,M
\end{aligned}
\tag{1}
$$

The model also needs to satisfy a linear static equation, where $\underset{\sim}{K}$ is the global stiffness matrix, $\underset{\sim}{u}$ is the displacement vector, and $\underset{\sim}{f}$ is the applied force vector. Both $\underset{\sim}{K}$ and $\underset{\sim}{u}$ depend on all design variables. There are total $2M$ constraints, where each constraint is imposed on a design space set N_i, with $\bar{M}_i$ as the upper bound for i-th mass fraction constraint, $\bar{Q}_i$ as the upper bound for the i-th joint cost fraction constraint, v_j is the volume of j-th element, and ρ^k is the density of the k-th material candidate. For the joining cost fraction constraint, q^k defines the joint cost of the k-th material candidate, and is only valid for the joint materials. The mass weighting factor w_j^k represents the amount of each k-th material candidate in each j-th element, with values ranging from 0 (void) to 1 (solid), and is interpolated from the design variables.

2.2 Material Interpolation

The interpolated Young's modulus E_j can be expressed as the weighted sum of Young's modulus of four material candidates in (2), where ω_j^k is the stiffness weighted factor for j-th element and k-th material, and E^k is the stiffness of the k-th material. In the converged result, each element should only contain one material, which means one weighting factor is 1 while the other three are 0. Intermediate densities are discouraged through a penalty factor p with values between 3 and 5. The interface existence variable n_j depends on the structural material distribution.

$$
\begin{aligned}
E_j(x_j^k) &= \sum_{k=1}^{4} \omega_j^k E^k \\
\omega_j^1 &= (1-n_j)(x_j^1)^p (x_j^2)^p \\
\omega_j^2 &= (1-n_j)(x_j^1)^p \left(1-(x_j^2)^p\right) \\
\omega_j^3 &= n_j (x_j^3)^p (x_j^4)^p \\
\omega_j^4 &= n_j (x_j^3)^p \left(1-(x_j^4)^p\right)
\end{aligned}
\tag{2}
$$

Similarly, (3) shows the interpolation for density and the expression for weighting factor w_j^k. Penalization is not needed here.

$$
\begin{aligned}
\rho_j(x_j^k) &= \sum_{k=1}^{4} w_j^k \rho^k \\
w_j^1 &= (1-n_j) x_j^1 x_j^2 \\
w_j^2 &= (1-n_j) x_j^1 (1-x_j^2) \\
w_j^3 &= n_j x_j^3 x_j^4 \\
w_j^4 &= n_j x_j^3 (1-x_j^4)
\end{aligned}
\tag{3}
$$

If all materials are isotropic and are assumed to have the same Poisson's ratio, then the interpolated element stiffness matrix $\underset{\sim}{K}_j(x_j^k)$ can be calculated using (4), where $\underset{\sim}{K}_j^k$ is the element stiffness matrix for solid candidate material.

$$
\underset{\sim}{K}_j(x_j^k) = E_j \frac{\underset{\sim}{K}_j^1}{E^1} = E_j \frac{\underset{\sim}{K}_j^2}{E^2} = E_j \frac{\underset{\sim}{K}_j^3}{E^3} = E_j \frac{\underset{\sim}{K}_j^4}{E^4}
\tag{4}
$$

The element stiffness matrix $\underset{\sim}{K}_j$ is resized into global dimension by inserting empty columns and rows at correct degrees of freedom. The global stiffness matrix $\underset{\sim}{K}$ is the summation of all resized matrices, $\underset{\sim}{K}_j^R$, including both designable and non-designable elements, N.

$$
\underset{\sim}{K} = \sum_{j\in N} \underset{\sim}{K}_j^R
\tag{5}
$$

2.3 Interface Detection

Interfaces between materials are identified through a spatial gradient calculation of the material selection design variable field $\underset{\sim}{x}^2$ using an unstructured approach [8]. The spatial gradient in the m-th spatial direction $\nabla_m x_j^2$ is calculated using (6), where h_{ji} is a distance term between the j-th and i-th element centroids and θ_{mji} is the angle between the m-th direction and a vector from

the *j*-th to the *i*-th element centroid. The summation is calculated over the N_j neighbouring elements within a search radius r. The magnitude of the spatial gradient is then calculated.

$$\nabla_m x_j^2 = \frac{1}{\sum_{i\in N_j} h_{ji} v_i} \sum_{i\in N_j} h_{ji} v_i \left(x_i^2\right)^p \cos\theta_{mji}$$
$$h_{ji} = \max\left(0, r - \mathrm{dist}(j,i)\right) \tag{6}$$
$$\left\|\nabla_m x_j^2\right\| = \sqrt{\sum_{m=1}^{3} \nabla_m x_j^2}$$

The spatial gradient magnitude is thinned and projected in (7) to calculate the final interface term used in the material interpolation schemes. The β projection parameter controls the slope and η controls the horizonal shift of the Heaviside function.

$$n_j = \frac{1}{1+e^{-2\beta\left[\left(1-x_j^2\right)\left\|\nabla_m x_j^2\right\|-\eta\right]}} \tag{7}$$

2.1 Sensitivity Analysis

Sensitivity for the total compliance including all designable and non-designable elements is shown in (8).

$$\frac{\partial C}{\partial x_j} = -\underset{\sim}{u}^T \frac{\partial \underset{\sim}{K}}{\partial x_j} \underset{\sim}{u} \tag{8}$$

The expression for the stiffness matrix can be derived as shown in (9).

$$\frac{\partial \underset{\sim}{K}}{\partial x_j} = \frac{\underset{\sim}{K}_j}{E_j} \frac{\partial E_j}{\partial x_j} \tag{9}$$

The sensitivity of the mass fraction and joint cost fraction constraints g_i^1 and g_i^2 is shown in (10).

$$\frac{\partial g_i^1}{\partial x_j} = \frac{1}{\sum_{l\in N_i} v_l \rho^1} \sum_{l\in N_i} \left(v_l \sum_{k=1}^{4} \frac{\partial w_l^k}{\partial x_j} \rho^k \delta_{lj} \right)$$
$$\frac{\partial g_i^2}{\partial x_j} = \frac{1}{\sum_{j\in N_i} v_j} \sum_{l\in N_i} \left(v_l \sum_{k=3}^{4} \frac{\partial w_l^k}{\partial x_j} q^k \delta_{lj} \right) \tag{10}$$
$$\delta_{lj} = \begin{cases} 1 & \text{if } l = j \\ 0 & \text{if } l \neq j \end{cases}$$

The sensitivities of the material, mass, and cost interpolation schemes, and for interface detection calculations are explained in detail in [7] and are not presented in this work.

3. RESULTS AND DISCUSSION

The MM-MJ-TO is implemented through in-house code using the MMA optimizer [9], with the FEA analysis performed in Altair OptiStruct.

3.1 Cantilever Beam

The 2D cantilever beam model is shown in Figure 1. The left edge is constrained in all degrees of freedom, and a force of 1000 N is applied on the middle node of the right edge in downwards direction. The geometry is discretized into 40 × 200 CQUAD4 elements. The left half of the model is design space 1 (DS 1) and the right half of the model is design space 2 (DS 2).

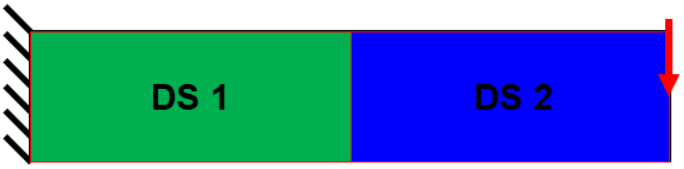

FIGURE 1: 2D CANTILEVER DESIGN SPACES AND BOUNDARY CONDITIONS

The two structural materials are titanium and aluminum, while the two joint materials are weld and adhesive. The material properties are shown in Table 1. The Poisson's ratio for all materials is set to be 0.3. In real life models, the joint interface regions are thinner than the element size, therefore homogenization is needed to approximate joint properties. Since the purpose of this paper is to demonstrate the methodology, the joints are assumed to be isotropic and with arbitrarily defined properties.

TABLE 1: MATERIAL PROPERTIES USED FOR CANTILEVER BEAM PROBLEM

Material Property	Titanium	Aluminum	Weld	Adhesive
Stiffness E^k (GPa)	110	70	50	30
Density ρ^k (g/cm^3)	4.5	2.7	3.6	2.4

Four case studies have been conducted with various mass fraction constraints without using any joint cost fraction constraints. The optimized results are shown in Figure 2. The amount of each material in the optimized geometry is reported as a mass fraction (MF) in percentage value calculated relative to a design space of solid titanium.

In case 1, the problem is solved with a single design space with a 30% mass fraction constraint on all elements. In case 2, both DS 1 and DS 2 are subjected to a 30% mass fraction constraint, resulting in an overall equivalent mass, but with an even distribution between the design spaces. In case 3 and 4, DS 1 and 2 are subjected to two combinations of 15% and 45% mass fraction constraints, resulting in an overall resultant mass fraction of 30%.

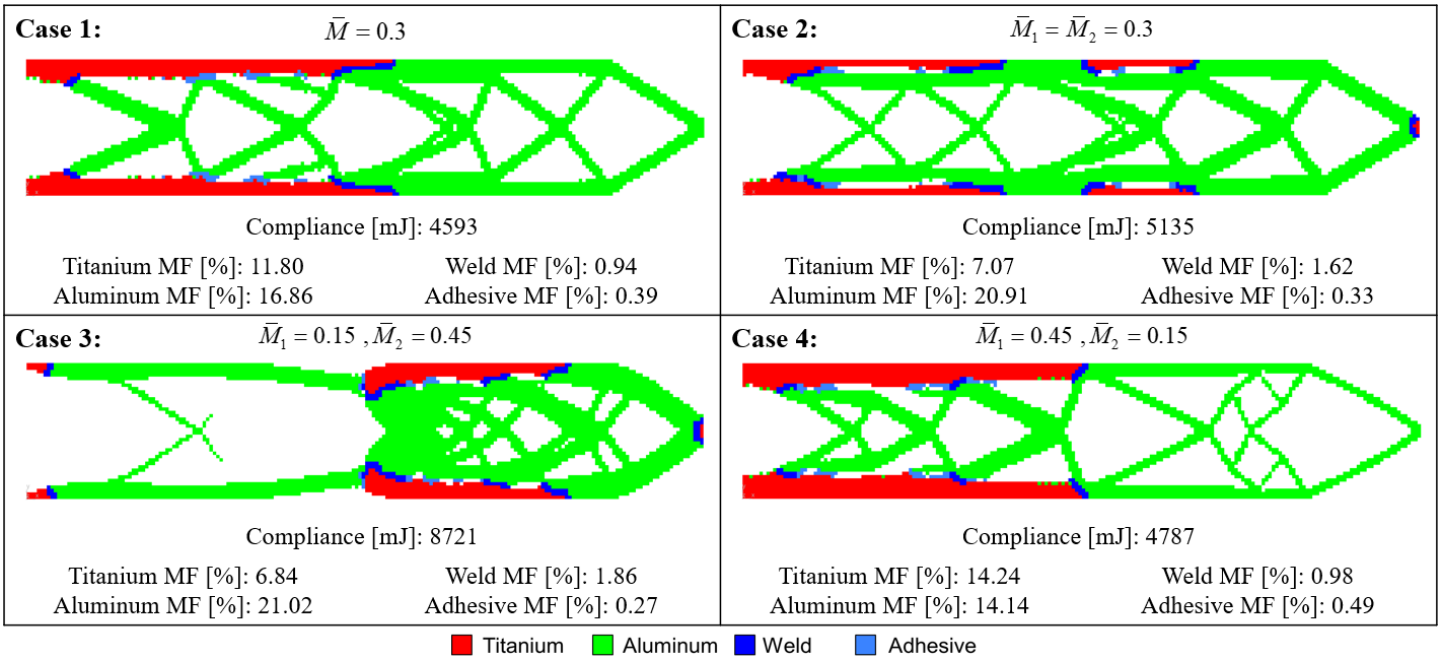

FIGURE 2: CANTILEVER BEAM CASE STUDIES DEMONSTRATING THE EFFECT OF VARYING MASS FRACTION (MF) CONSTRAINT LIMITS

Titanium, the stronger material, is placed on the top and bottom sides of the cantilever beam (and the load applied location in some cases), because these regions have high compliance and need to be reinforced. All joints are located between titanium and aluminum, which is expected.

Case 1 has 11.8% better objective (compliance) than case 2 because the additional mass fraction constraint in case 2 reduces the design freedom. However, case 2 has a more uniform distribution of material. Case 3 has the worst objective because less material is placed on the left where the bending stress is highest and should be strengthened. Case 4 has a similar objective value and topology to case 1.

Design space mass fraction constraints influence the material distribution and the usage of joints within the structure. For example, Case 2 and Case 3 require more joints because there are five distinct titanium regions present in the solution (compared to two distinct regions in Case 1), even though the mass of titanium is smaller in Case 2 and Case 3.

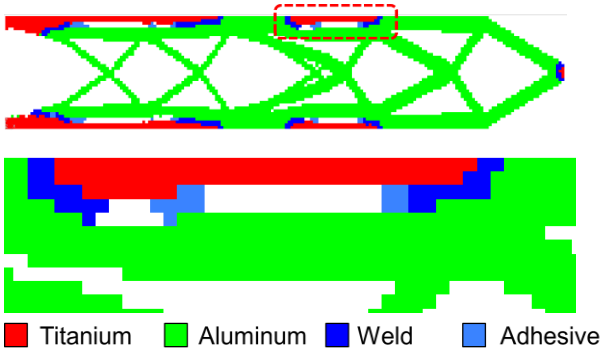

FIGURE 3: PLACEMENT OF JOINT MATERIALS IN MULTI-MATERIAL CONNECTION UNDER TENSILE LOAD

Figure 3 shows a closeup view of a tension member from Case 2 result. Most of weld (the stiffer joint) is placed near the end points of the titanium member, while adhesive joints are placed closer to the middle. This configuration is efficient for transferring tension load between titanium and aluminum members.

3.2 Truck Chassis Frame

The proposed method is applied to a truck chassis frame model to demonstrate its effectiveness on practical problems with complex loading and geometry. In addition, joining cost fraction constraints are introduced to this problem. The model shown in Figure 4 is meshed using approximately 180,000 hexahedral elements with side lengths of about 30mm divided into three design spaces (DS). DS 1, DS 2, and DS 3 represent the frame, cab, and bed of the truck, respectively, which are typically manufactured and assembled individually before a final assembly stage. This division of the geometry allows for the overall structure to be optimized while providing more control over the mass and joining cost in specific regions. It is important to note this model does not have a small enough element size to generate any small-scale features of the truck assembly and should instead be used as a first step in the conceptual design process to identify material distribution, followed by further stages of optimization on individual components with a refined mesh.

A unique load is applied in 35 different load steps, each with an arbitrary magnitude of 1000 N distributed using RBE3 elements. The four points representing the wheels are connected using an RBE3 element to a single central node that is constrained in all degrees of freedom.

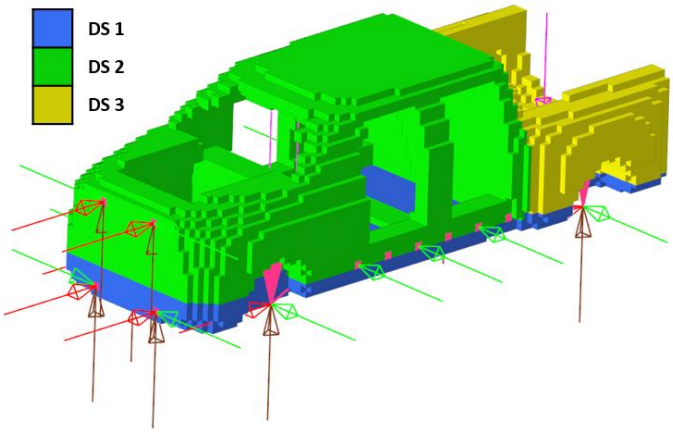

FIGURE 4: FINITE ELEMENT MODEL FOR TRUCK CHASSIS FRAME WITH THREE DESIGN SPACES (DS)

The truck chassis frame problem is solved using steel and aluminum candidate materials, as well as weld and adhesive joint candidate materials. The associated material properties are summarized in Table 2. As with the cantilever beam problem, the Poisson's ratio for all materials is set to 0.3 and approximate joint properties are determined assuming homogenized material properties along interface elements. Joint cost values are arbitrarily defined with a value of 2 for welds and 1 for adhesives. These values represent a relative magnitude of joining cost between candidate joint materials, and therefore the exact values of joining cost are not physically meaningful.

TABLE 2: MATERIAL PROPERTIES USED FOR TRUCK CHASSIS FRAME PROBLEM

Material Property	Steel	Aluminum	Weld	Adhesive
Stiffness E^k (GPa)	210	70	112	42
Density ρ^k (g/cm^3)	7.85	2.7	5.3	4.2
Joint Cost q^k ($/cm^3)	-	-	2	1

As shown in Case 1 of Figure 5, the truck model was first solved without joint cost constraints using mass fraction values of 10% for DS 1 and DS 3 and 30% for DS 2. This solution placed steel around all load application points due to the high compliance in these regions. In addition, steel regions connect the two bottom steel members beneath the middle of the passenger compartment and reinforce from the front to back of the truck chassis through the A and C pillars. In this problem statement without cost, welds are placed at all interfaces between the steel and aluminum components.

In Case 2, a loose joint cost fraction constraint of 10% is introduced for DS 1 and DS 3 and a tight joint cost fraction constraint is assigned to DS 2. The joint cost fraction constraint functions as a volume fraction constraint applied only to joint materials, with different cost weighting factors applied as per Table 2. The optimized result in Case 2 has a similar structure to Case 1 in DS 1 and DS 3, as the joint cost constraints are not limiting the design ($g_1^2 = 0.046$, $g_3^2 = 0.048$). In DS 2, the distribution of steel and aluminum is similar to Case 1, while the

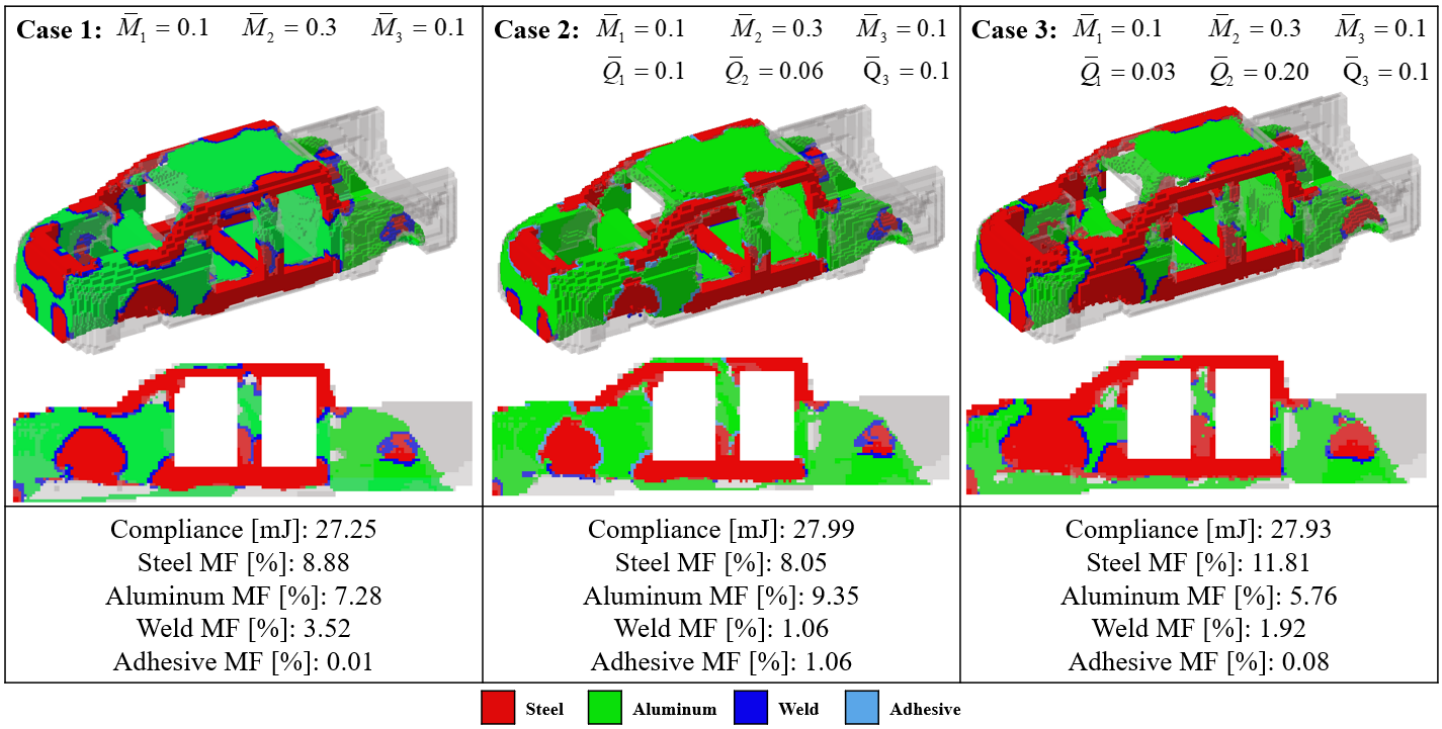

FIGURE 5: OPTIMIZATION RESULTS FOR TRUCK CHASSIS FRAME STUDY WITH VARYING JOINT COST FRACTION CONSTRAINT

joint distribution is changed drastically to meet the cost fraction constraint. Joint elements are removed from many of the interface regions (indicating no connection to be used in that location) and adhesives instead of welds are used to connect between structural materials. The additional constraint results in a 3% increase in compliance compared to Case 1. Looking at the mass fractions of these designs, Case 2 uses 70% less weld material and increases the adhesive use to satisfy the joining cost constraint. The structural material distribution also changes with a 28% increase in aluminum in Case 2.

The final problem statement in Case 3 uses a strict joint cost constraint of 3% in DS 1 and looser joint cost constraints in DS 2 and DS 3. In this case, the optimization converges to a different distribution of structural material, with more aluminum material added beneath the engine area. There is also 30% more steel used compared to Case 1, with the majority added to DS 1. These changes occur because the optimization converges to a different local optimum solution. The changes to DS 1 are highlighted in Figure 6. Note that the floating elements shown in Case 3 are connected to material from the design spaces hidden from this image.

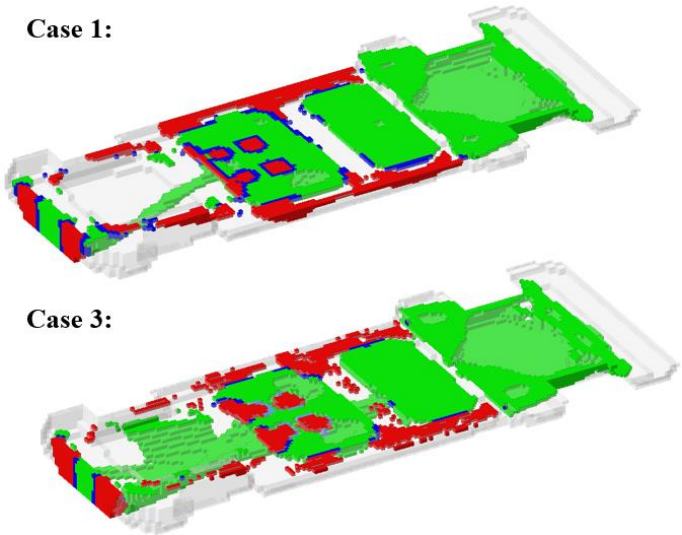

FIGURE 6: COMPARISON OF TRUCK BED STRUCTURE IN DS 1 FOR CASE 1 AND CASE 3 RESULTS

4. CONCLUSION

This work presents a multi-material and multi-joint topology optimization methodology with the capability to restrict mass and cost fraction across multiple design spaces. The approach was applied on an academic cantilever beam problem to show the implications of using more than one design space in MM-MJ-TO problems. The truck chassis frame model demonstrates the effectiveness of this approach to reduce the joining material in specific regions of the geometry.

In terms of future work, the interface between the design space and non-design space should be considered. Adding the capability to consider manufacturing constraints, such as extrusion, symmetry, or casting, would further improve the manufacturability of the design. Additionally, supporting more optimization problem statements, with the inclusion of displacement or stress constraints, would expand the scope of the tool.

REFERENCES

[1] Bendsøe, Martin Philip and Kikuchi, Noboru. “Generating optimal topologies in structural design using a homogenization method.” *Computer Methods in Applied Mechanics and Engineering* Vol. 71 No. 2 (1988): pp. 197–224. DOI 10.1016/0045-7825(88)90086-2.

[2] Bendsøe, Martin Philip. “Optimal shape design as a material distribution problem.” *Structural Optimization*, Vol. 1 No. 4, (1989): pp. 193–202. DOI 10.1007/BF01650949.

[3] Shah, Vishrut, Pamwar, Manish, Sangha, Balbir and Kim, Il Yong. “Material interface control in multi-material topology optimization using pseudo-cost domain method.” *International Journal for Numerical Methods in Engineering* Vol. 122 No. 2 (2020): pp. 455–482. DOI 10.1002/nme.6545.

[4] Woischwill, Christopher and Kim, Il Yong. “Multimaterial multijoint topology optimization.” *International Journal for Numerical Methods in Engineering* Vol. 115 No. 13 (2018): pp. 1552–1579. DOI 10.1002/nme.5908.

[5] Florea, Vlad, Pamwar, Manish, Sangha, Balbir and Kim, Il Yong. “3D multi-material and multi-joint topology optimization with tooling accessibility constraints.” *Structural and Multidisciplinary Optimization* Vol. 60 No. 6 (2019): pp. 2531–2558. DOI 10.1007/s00158-019-02344-1.

[6] Florea, Vlad, Pamwar, Manish, Sangha, Balbir and Kim, Il Yong. “Simultaneous single-loop multimaterial and multijoint topology optimization.” *International Journal for Numerical Methods in Engineering* Vol. 121 No. 7, (2020): pp. 1558–1594.

[7] Crispo, Luke, Roper, Stephen William Knox, Bohrer, Rubens, Morin, Rosalie and Kim, Il Yong. “Multi-material and multi-joint topology optimization for lightweight and cost-effective design.” *Proceedings of the ASME IDETC/CIE*. DETC2021-67317. Virtual, Online, August 17–19, 2021. DOI 10.1115/DETC2021-67317.

[8] Crispo, Luke, Bohrer, Rubens, Roper, Stephen William Knox and Kim, Il Yong. “Spatial gradient interface detection in topology optimization for an unstructured mesh.” *Structural and Multidisciplinary Optimization* Vol. 63 No. 1 (2021): pp. 515–522. DOI 10.1007/s00158-020-02688-z.

[9] Svanberg, Krister. “The method of moving asymptotes–a new method for structural optimization.” *International Journal for Numerical Methods in Engineering* Vol. 24 No. 2 (1987): pp. 359–373. DOI 10.1002/nme.1620240207.